Geophysical Research Letters

RESEARCH LETTER
10.1029/2024GL109492

Formation Mechanisms of Large-Scale Folding in Greenland's Ice Sheet

Yu Zhang[1], Till Sachau[1], Steven Franke[1,2], Haibin Yang[3], Dian Li[1,4], Ilka Weikusat[1,2], and Paul D. Bons[1,5]

[1]Department of Geosciences, Tübingen University, Tübingen, Germany, [2]Alfred Wegener Institute, Helmholtz Centre for Polar and Marine Research, Bremerhaven, Germany, [3]School of Earth Sciences, Zhejiang University, Hangzhou, China, [4]College of Earth and Planetary Science, Chengdu University of Technology, Chengdu, China, [5]School of Earth Science and Resources, China University of Geosciences (Beijing), Beijing, China

Key Points:

- Large-scale fold formation in polar ice sheets is mainly controlled by ice anisotropy and bedrock topography
- Buoyancy of deep warm ice can further enhance fold amplification
- The implementation of ice anisotropy should be included in large-scale ice flow modeling

Supporting Information:

Supporting Information may be found in the online version of this article.

Correspondence to:

Y. Zhang and P. D. Bons,
yu.zhang@mnf.uni-tuebingen.de;
paul.bons@uni-tuebingen.de

Citation:

Zhang, Y., Sachau, T., Franke, S., Yang, H., Li, D., Weikusat, I., & Bons, P. D. (2024). Formation mechanisms of large-scale folding in Greenland's ice sheet. *Geophysical Research Letters*, *51*, e2024GL109492. https://doi.org/10.1029/2024GL109492

Received 5 JUN 2024
Accepted 14 AUG 2024

Author Contributions:

Conceptualization: Yu Zhang, Paul D. Bons
Data curation: Steven Franke
Methodology: Yu Zhang, Till Sachau, Dian Li
Project administration: Ilka Weikusat, Paul D. Bons
Software: Haibin Yang
Writing – original draft: Yu Zhang
Writing – review & editing: Till Sachau, Steven Franke, Haibin Yang, Paul D. Bons

Abstract Radio-echo sounding (RES) shows large-scale englacial stratigraphic folds are ubiquitous in Greenland's ice sheet. However, there is no consensus yet on how these folds form. Here, we use the full-Stokes code Underworld2 to simulate ice movements in three-dimensional convergent flow, mainly considering ice anisotropy due to a crystallographic preferred orientation, vertical viscosity and density gradients in ice layers, and bedrock topography. Our simulated folds show complex patterns and are classified into: large-scale folds (>100 m amplitude), small-scale folds (<<100 m) and basal-shear folds. The amplitudes of large-scale folds tend to be at their maximum in the middle of the ice column or just below, in accordance with observations in RES data. We conclude that ice anisotropy amplifies the perturbations in ice layers (mainly due to bedrock topography) into large-scale folds during flow. Density differences between the warm deep ice and cold ice above may enhance fold amplification.

Plain Language Summary Polar ice sheets are composed of compacted former snow layers deposited at the ice surface. If not distorted or deformed, these layers are flat or adapt to the underlying bedrock topography. However, vertical radar scans of Greenland's ice sheet show large-scale folds of up to hundreds of meters in height. To investigate how these large-scale folds form, we set up a three-dimensional numerical ice-sheet model and simulate fold growth. Our modeling emphasizes the distinctive physical properties of ice required for fold formation, notably its anisotropy (the direction dependency of the flow strength) and power-law rheology (when ice becomes softer with increasing strain rate). These findings help to better explain ice flow dynamics.

1. Introduction

Airborne radio-echo sounding (RES) data reveal internal layering and large-scale folding (up to >100 m, sometimes even 1 km fold amplitude) on the bumpy bedrock in several regions of Greenland's ice sheet (GrIS, Figure 1) (Bell et al., 2014; Bons et al., 2016; Franke, Bons, et al., 2022, Franke, Jansen, et al., 2022; Jansen et al., 2024; Leysinger Vieli et al., 2018; MacGregor et al., 2015; NEEM community members, 2013; Panton & Karlsson, 2015; Wolovick et al., 2014). Large-scale folds appear both within ice streams and in regions of slow-moving ice. Fold amplitudes usually reach their maximum in the middle of the ice column or just below, gradually decrease toward the upper layers and flatten at the ice surface. Studies of past and present ice dynamics (Franke, Bons, et al., 2022) and of basal conditions (Leysinger Vieli et al., 2018; Wolovick et al., 2014) need to include mechanisms to generate folds to be robust. Fold geometry can be used to date the establishment of shear margins of ice streams (Jansen et al., 2024) and is needed to unravel ice stratigraphy in ice cores that penetrate folded ice (NEEM community members, 2013).

Several mechanisms and models have been proposed to explain the formation of folds in ice sheets. Bell et al. (2014) and Leysinger Vieli et al. (2018) suggest that refreezing meltwater adds material to the ice base and elevates the overlying stratigraphy and influences basal ice deformation. Alternatively, Wolovick et al. (2014) suggest that variable slip rates due to "traveling slippery patches" can create large-scale folds. Furthermore, Krabbendam (2016) proposes the basal temperate (melting) ice layer may be locally thickened by internal deformation of folding or thrusting over a bedrock high. These models mainly focus on basal ice and bed conditions, which may apply to individual fold cases but seem inadequate to explain the presence of folds throughout the GrIS, especially in the NE of the ice sheet. Additionally, these models are purely 2D along-flow models and no

10.1029/2024GL109492

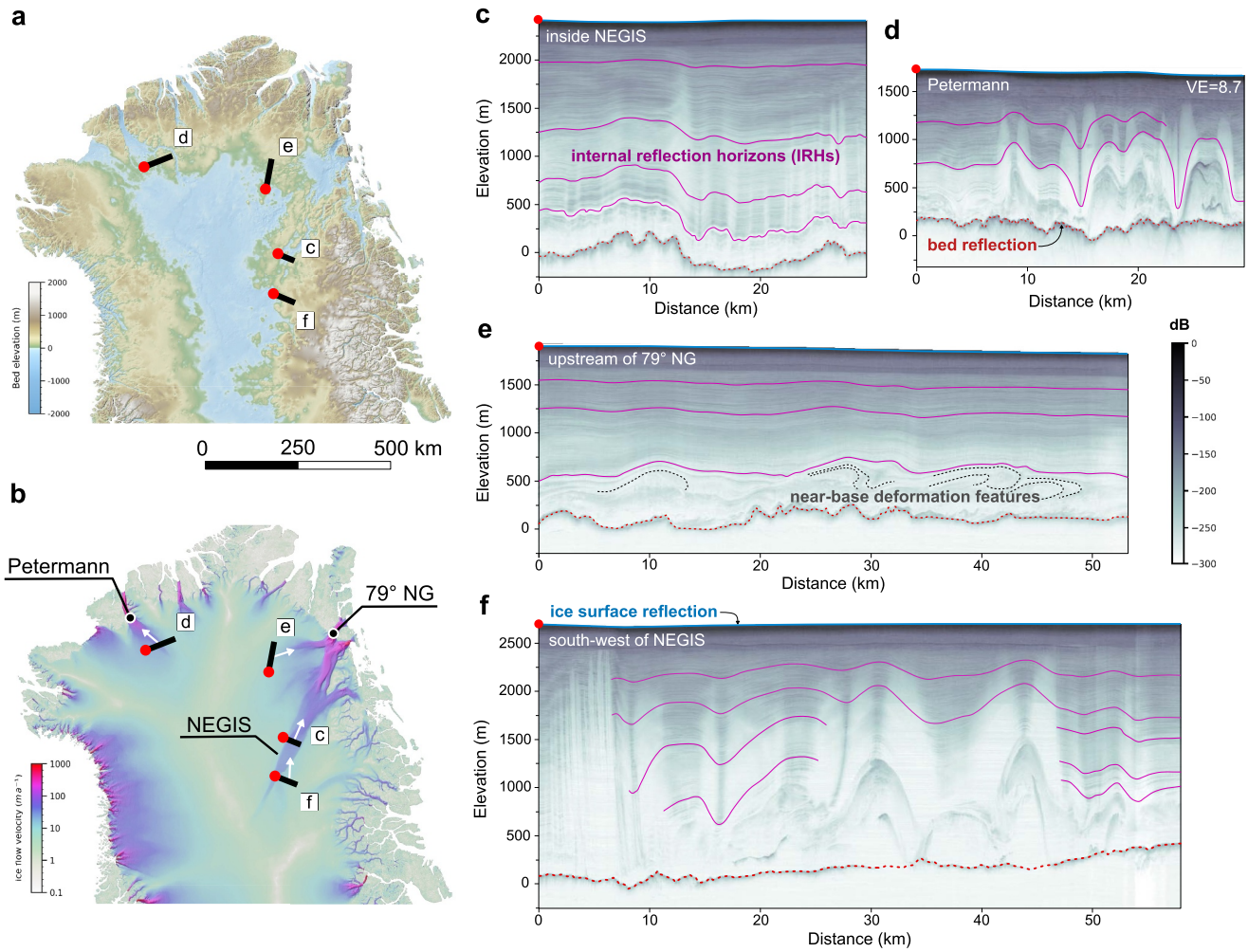

Figure 1. Overview of the northern Greenland ice sheet and radio-echo sounding (RES) profiles: (a) bedrock topography (Morlighem et al., 2017) and location of RES profiles; (b) ice surface flow velocity (Joughin et al., 2018) and the average flow direction relative to the profiles (white arrows) (c–f) RES images (Franke, Bons, et al., 2022, Franke, Jansen, et al., 2022) showing englacial folds (c) in the central North-East Greenland Ice Stream (NEGIS), (d) at the Petermann ice stream, (e) upstream of the 79° North Glacier (Nioghalvfjerdsbrae), and (f) in the upstream region of the NEGIS. Note the strong vertical exaggeration (8.7×) in the RES-profiles.

predictions have been published for their 3D geometry. However, especially when considering the margins of ice streams, the three-dimensional geometries of folds show that fold axes are sub-parallel or at a small angle to the flow direction (Bons et al., 2016; Franke, Bons, et al., 2022, 2023).

Hudleston (2015) proposes that irregularities in primary ice stratification can be kinematically amplified in convergent flow by horizontal shortening and without the requirement of rheological contrast in the ice. Thorsteinsson and Waddington (2002) invoke anisotropy as a cause of fold initiation near ice-sheet centers considering the initial layer disturbance relative to the extensile flow regime, and anisotropy is also well-studied in the development of small-scale folds in ice cores (Alley et al., 1997; Jansen et al., 2016) and anisotropic materials (Kocher et al., 2008; Ran et al., 2019). Bons et al. (2016) and Jansen et al. (2024) suggest that mechanical anisotropy and convergent flow cause large-scale folding. This hypothesis has so far not been tested with numerical simulations.

Three properties of ice or ice sheets are significant for the modeling of flow in ice sheets: (a) The viscoplastic deformation of ice I_h (hexagonal ice) results essentially from dislocation glide parallel to the crystallographic basal plane (Gillet-Chaulet et al., 2006). The crystallographic preferred orientation (CPO) in ice sheets is typically a vertical alignment of the crystals' c-axes, which are perpendicular to the easy-glide basal planes. As a result, the ice becomes significantly anisotropic in its flow properties (Duval et al., 1983). (b) Ice temperature increases with

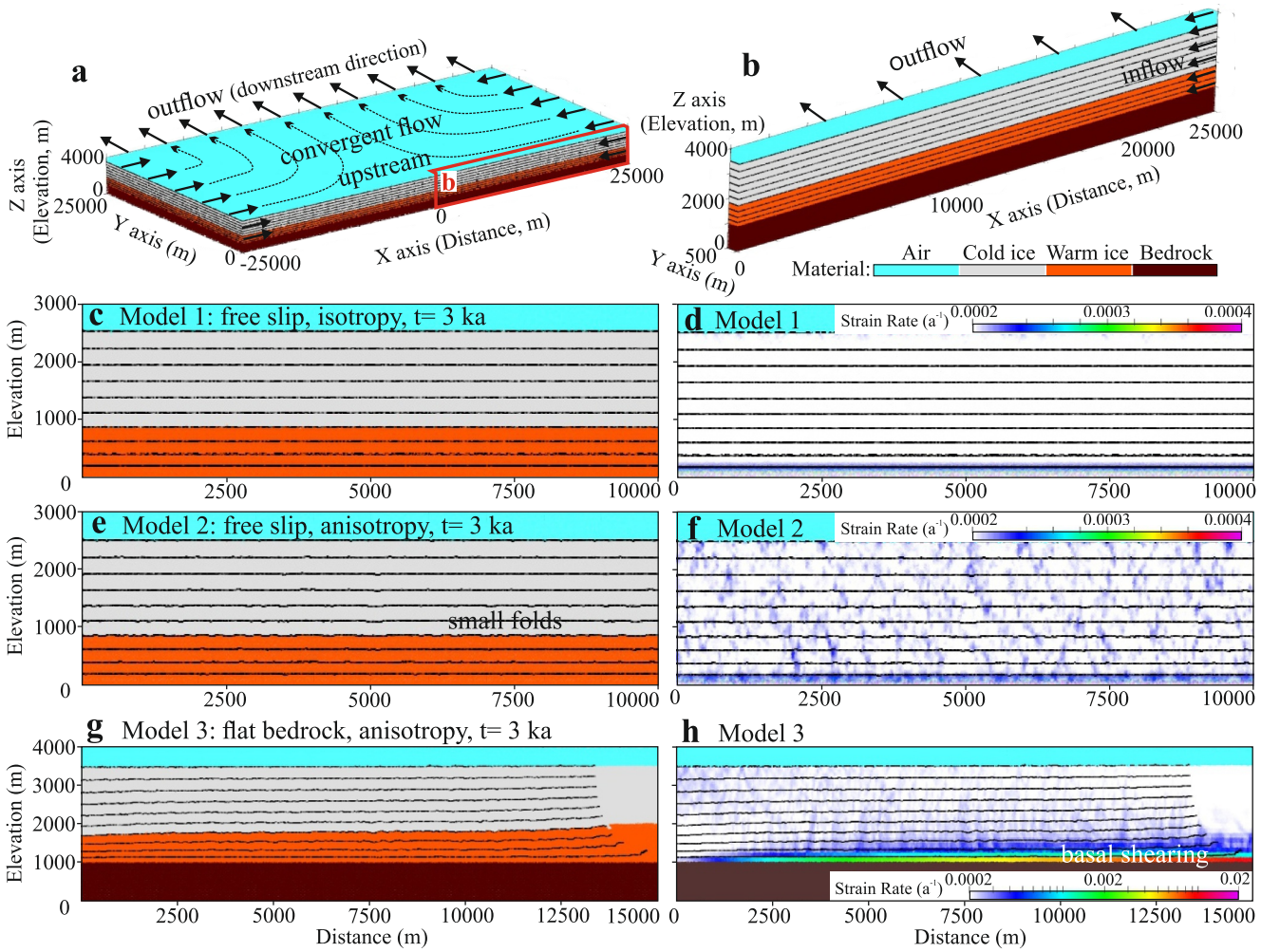

Figure 2. Model design and snapshots of results from Models 1–3 after 3,000 years: (a) 3D view of initial model (example from flat bedrock model) and (b) the adapted model to enable a higher model resolution (see location in Figure 2a) (c–h) profile snapshots of the layer geometry and the second invariant of strain-rate magnitude parallel to x-z coordinate plane (at y = 250 m, same in Figures 3 and 4) for (c–d) Model 1, (e–f) Model 2 and (g–h) Model 3.

depth: upper "cold ice" has a high viscosity and density, while the lower "warm ice" has a lower viscosity and also has a lower density due to thermal expansion (Robin, 1955; Rogozhina et al., 2011). Hughes (2009) proposes the thermal convection hypothesis and the possibility of fold formation. (c) Ice layers are initially not necessarily perfect sheets with constant thickness. The irregularities may come from the ice divides (Thorsteinsson & Waddington, 2002), variable basal processes (Leysinger Vieli et al., 2018; Wolovick et al., 2014), and more generally the underlying bedrock topography (Figure 1c; Hudleston, 2015). In addition, not all layering is necessarily strained original stratigraphy. Layers could be created by the deformation process, especially when strain is high (Jennings & Hambrey, 2021). Taking these considerations into account, we here use the full-Stokes software "Underworld2" (Beucher et al., 2022; Sachau et al., 2022) to investigate the development of folds in 3D convergent flow. We investigate particularly the factors rheological anisotropy of ice, vertical gradients of viscosity and density, and bedrock topography.

2. Method

The basic model design is shown in Figure 2a (detailed parameters in Text S1, Table S1 and Figures S1–S2 in Supporting Information S1). The model comprises four main material layers: air (500 m), cold ice (1,667 m; −30°C), warm ice (833 m; −30 to −3°C), and bedrock, and 10 internal marker horizons to track the deformation. Internal horizons are progressively shortened by lateral inflows (x-axis) of 5 m/yr. To reduce computing time, our model (Figure 2b) thus consists of one half of a convergent zone (Figure 2a), as, for example, envisaged by Bons

10.1029/2024GL109492

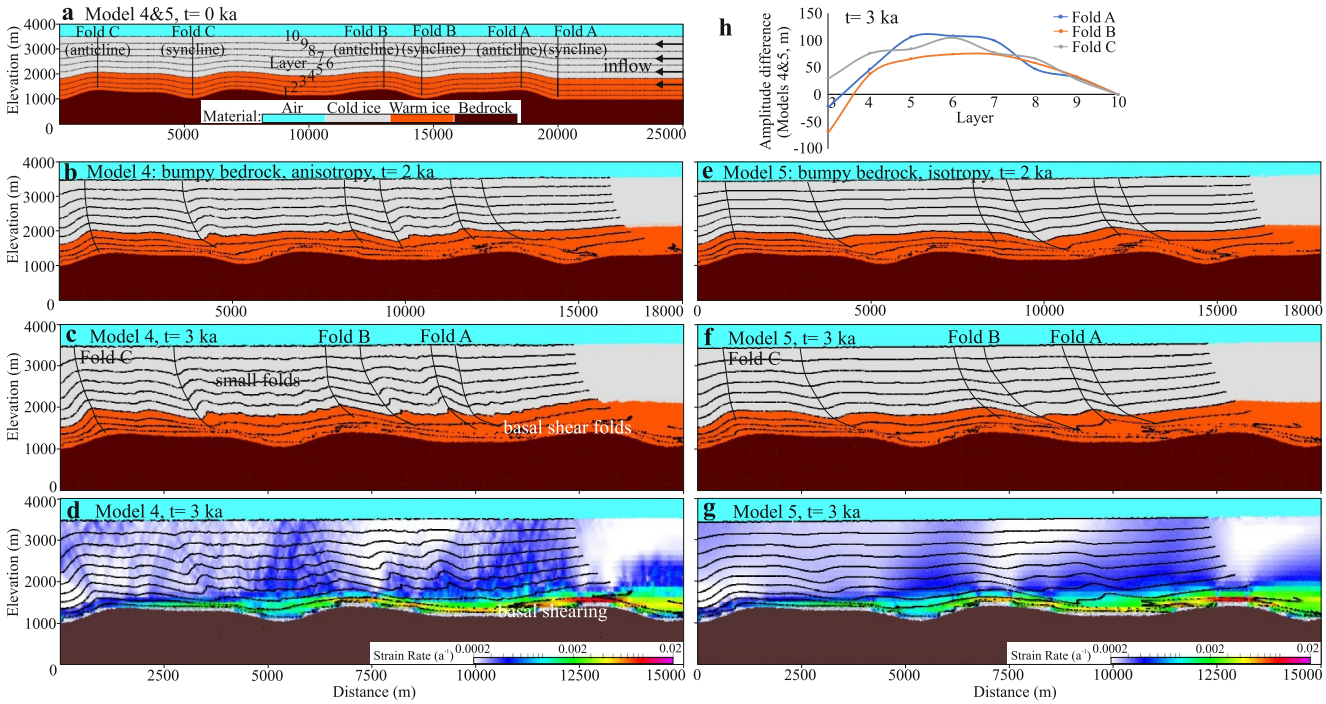

Figure 3. Snapshots of comparison of anisotropic Model 4 and isotropic Model 5 with identical bedrock topography with 400 m tall bumps in both models shown in (a): (b–c) Layer geometry snapshots of Model 4 after (b) 2,000 years and (c) 3,000 years. (d) The second invariant of strain-rate magnitude in Model 4 at 3,000 years. (e–f) Layer geometry snapshots of Model 5 after 2,000 and 3,000 years. (g) The second invariant of strain-rate magnitude for Model 5 after 3,000 years. Note that the *x*-axis and *z*-axis scales between the images of individual time steps. (h) Amplitude differences between Models 4 and 5 of Layers 3–10 on Fold A, Fold B and Fold C after 3,000 years.

et al. (2016) for the inlet area of the Petermann Glacier. Outflow in the y-directon, compensates the inflow to maintain a constant ice volume. As the main interest is in the ice-layer geometry in the vertical x-z-plane, and to maximize the resolution of the model, its width in the *y*-direction (500 m) is much smaller than in the *x*-direction (25 km). A 25 × 25 km model is shown in Figures S7–S8 in Supporting Information S1 for comparison.

The non-linear viscous ice rheology used is the dislocation creep component of the Goldsby and Kohlstedt (2001) composite flow law. The flow law has two parameterizations, one for high and one for low temperature, and the parameters used are those modified by Kuiper et al. (2020) to ensure no discontinuity at the transition temperature (−11°C). The power-law viscosity of ice (isotropic viscosity η_1, Pa · s) is derived from temperature (T, °C) and strain rate ($\dot{\varepsilon}_{ij}$, yr^{-1}). Underworld2 is a particle-in-cell model and the local c-axis orientations are stored for each particle. Initial c-axis orientations of ice particles are perpendicular to the local layer orientation with a Gaussian random distribution with a standard deviation of ±5°. As the simulation progresses, the c-axes rotate in the flow field (Sharples et al., 2016). The anisotropy of the ice crystal is modeled as transverse isotropic (Martín et al., 2009; Sharples et al., 2016) by two viscosity values: a maximum value η_1 (Pa · s) for shortening or stretching parallel to the c-axis maximum, and a minimum viscosity η_2 (Pa · s) for shearing along the plane perpendicular to the c-axis maximum. We define the intensity of anisotropy with the anisotropy parameter $k = \eta_1/\eta_2$.

Seven models are discussed here to explore the effect of the ice anisotropy, viscosity and density, and bed conditions on large-scale folding. Three different bed conditions are tested: (a) a free-slip bottom boundary without a bedrock (Figures 2c–2f), (b) a 1,000 m thick bedrock layer with a flat surface to which the ice is frozen (Figures 2g and 2h), and (c) the same as (b), but with an undulating bedrock surface with bumps of variable wavelengths and amplitudes (Figure 3). Internal horizons are parallel to bedrock bumps at the base of the ice. Amplitudes of bedrock-related undulations in the ice horizons decrease to zero at the ice surface (Figure 3a). In these models (see detailed comparisons in Table S2 in Supporting Information S1), we varied the following parameters: (a) bed condition (i) for Models 1–2, bed condition (ii) for Model 3, and bed condition (iii) (variable amplitude bumps up to 400 m) for Models 4–7; (b) isotropic ice for Model 1, Model 5 and Model 7, and anisotropic ice for all other models; (c) softness in ice viscosities (adapted A_0 value) for Models 6–7.

3. Results

3.1. Anisotropy Versus Vertical Viscosity and Density Gradients

In the simulations of isotropic ice on a free-slip bottom boundary (Model 1), ice layers stay nearly flat for at least 3,000 years, even with vertical viscosity and density gradients (Figures 2c and 2d). Nevertheless, when anisotropy is included in the models, a large number of small folds form (Model 2; Figures 2e and 2f), due to the Gaussian variability of the c-axis orientation of particles. Compared to the very homogeneous strain rates resulting from the isotropic Model 1 (Figure 2d), the strain-rate map of Model two is much more heterogeneous with zones of elevated strain rates (Figure 2f). In the scenario where the bedrock is added as a horizontal flat layer underneath the anisotropic ice (Model 3; Figures 2g and 2h) bedrock-parallel shearing occurs in the basal ice layers as the ice is frozen to the bedrock. Due to strain-rate softening, this enhances the vertical viscosity contrasts between the ice layers (Figure S6 in Supporting Information S1). However, no large-scale folds form, but instead abundant small folds similar to Model 2.

3.2. Anisotropic Versus Isotropic Ice on the Bumpy Bedrock

For the scenario with a bumpy bedrock topography (anisotropic Model 4), the initial ice layers on bedrock bumps start to evolve into large-scale folds (up to 300 m amplitude in 2,000–3,000 years) with additional small folds in between (Figures 3a–3d). Here we compare three large-scale fold sets A, B, and C in the anisotropic Model 4 and isotropic Model 5 (Figure 3), in terms of the fold amplitudes as a function of layer height. Amplitude is here defined as the difference in elevation of a marker horizon at a fold crest and adjacent trough (Jansen et al., 2024). We consider 10 stratigraphic layers labeled 1–10 from bottom to top (Figure 3a). The amplitude-layer values of Layers 3–10 are shown in Figure S5 in Supporting Information S1 (note that Layers 1–2 are too close to the bedrock and therefore strongly sheared). In Model 4, the amplitude of the initial layer depth variation is largest in the near-base layers and zero at the ice surface. The largest fold amplitudes are in middle layers (Layers 4–6) and mostly exceed the initial depth variation. In the isotropic Model 5 we observe large-scale folds that are inherited from the initial depth variation. They are smaller and without small folds in between (Figures 3e–3g). Folds with the largest amplitudes are found in the deepest layers, and amplitudes of most folds are smaller than the initial depth variation. Strain rates in Model 5 are high close to the ice base, decrease toward the ice surface in the upper layers and are distributed in a regular pattern associated with bedrock bumps (Figure 3g).

Considering ice flowing over variable bedrock bumps, folds do not always show monotonic growth over time in Model 4. The only difference in the settings between Models 4 and 5 is the anisotropy in the ice, thus we analyze the anisotropy contribution to fold growth by subtracting the fold amplitude (fold sets A, B and C) of the isotropy model (Model 5) from that of the anisotropy model (Model 4). After 3,000 years (Figure 3h), the amplitude differences between Models 4 and 5 of most folded layers are larger than 0 m, indicating that anisotropy does amplify folds after this period. The maximum amplification of over 100 m is in the middle layers (Layers 5–7).

3.3. Anisotropy and Buoyancy Effects Along the Outflow Direction

The outflow velocity in the stretching (y) direction in the semi-2D (Figure 2b) models is only 0.1 m/yr, which is comparable to flow velocities near the divide of the ice sheet. Further away from the divide horizontal flow velocities are much higher and bedrock-parallel shear rates are thus also higher. This effectively softens due to the strain-rate softening of the power-law viscous material. The effect can be seen in the 3D model (Figure 2a) in Figures S7–S8 in Supporting Information S1, where the outflow velocity is 5 m/yr. The strain-rate softening results in a decrease in effective viscosity and an increase in fold amplitudes in the outflow direction. This effect is simulated with Models 6 and 7 that has the same settings as Model 4 (Figure 3a), but we reduced the value of A_0 to reduce the effective viscosity by a factor of 30 to model the ice further downstream from the divide (See Table S1 Note in Supporting Information S1). Model six is for anisotropic ice and Model 7 for isotropic ice. Folds in the anisotropic Model 6 can reach over 500 m (to 987 m) in amplitude in only 1,000 years (Figure 4a), much larger (by up to 665 m) compared to the isotropic Model 7 (Figure 4b). Folds in both models grow faster compared to Models 4–5, and the most intensely folded layer of the fold sets is at the warm-cold ice interface (Layer 4), indicating the buoyancy effect of the lowermost warmer and strain-rate softened ice.

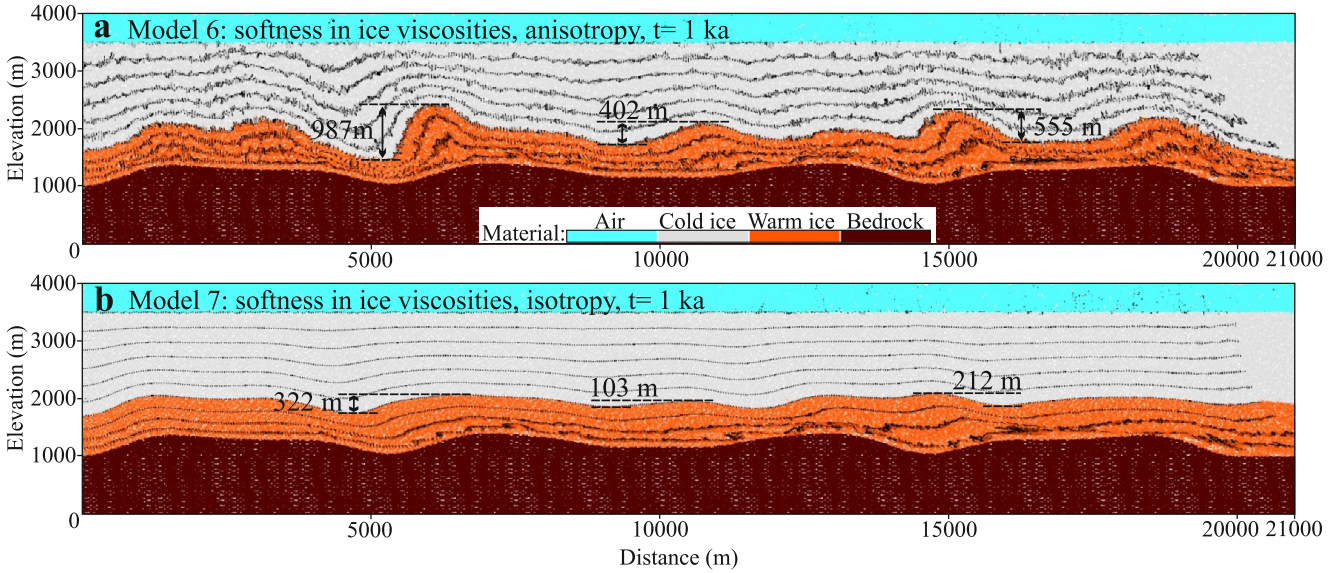

Figure 4. Layer geometry snapshots after 1,000 years of (a) anisotropic Model 6 with adapted A_0 value for softness in ice viscosities (near-downstream) and (b) isotropic Model 7 for comparison.

4. Discussion

The folds observed in our modeling can be classified into three types: large-scale folds (fold amplitudes >100 m), small-scale folds (fold amplitudes <<100 m, wavelength << km) and recumbent basal-shear folds. The large-scale folds have wavelengths in the order of one km or more. Their axial planes have a listric shape, with steep dips near the ice surface that become shallower toward the bedrock. Our simulated large-scale folds (in particular those in Models 4 and 6) show strong similarity to those observed in the GrIS by for example, Wolovick et al. (2014), MacGregor et al. (2015), Bons et al. (2016), Franke, Bons, et al. (2022) and Jansen et al. (2024) (Figure 1).

The main controlling factors for large-scale folds in our simulations are ice anisotropy and the initial geometry dictated by the underlying bedrock topography. Folds in isotropic ice ($k = 1$) (Figures 3e–3g) are essentially palimpsests of the underlying bedrock topography that are passively transported away from the underlying bumps. They do not amplify by themselves, but passively change their shape as they travel over bedrock bumps and valleys. In the anisotropic model with $k = 3$ (Figures 3b–3d), we observed additional fold-shape modification and amplification with ice c-axis rotation (Figure S4 in Supporting Information S1). When k is set to 6, this effect is even stronger (Figures S10 and S12 in Supporting Information S1). This is a clear indication that the anisotropy plays a primary role in fold amplification. This anisotropy effect could be more pronounced in real ice sheets, considering the higher anisotropy values proposed by Duval et al. (1983). Buoyancy becomes a significant factor to further enhance fold amplification if overall deformation of the ice sheet is fast enough to cause a general strain rate softening of the ice.

According to classical fold theory (Biot, 1957; Schmalholz & Mancktelow, 2016) folds form by the amplification of small perturbations in the folding layer. In case of folding of a strong layer in a softer matrix, a dominant wavelength will develop as a function of layer thickness (the characteristic length scale of the system) and the viscosity ratio of the layer and matrix. The dominant wavelength is the wavelength with the highest amplification rate. In case of a single, but anisotropic medium, a characteristic length scale is absent. As a consequence there is no dominant wavelength that amplifies the most, and folds of all wavelengths may form simultaneously, including small-scale folds (Figure 2e). Bedrock topography or variations in bed sliding and/or freezing/thawing (Leysinger Vieli et al., 2018; Wolovick et al., 2014) at the base of the ice sheet create seed folds that may subsequently amplify. With these, the system can "skip" the initial fold nucleation stage for folds with these wavelengths. These folds amplify depending on the intensity of the anisotropy (k) and overall strain rate and concomitant strain-rate weakening to enable buoyancy effects. However, in case of anisotropy small-scale folds will also nucleate due to small-scale perturbations (here the random noise in c-axis orientations).

In our models, the lowermost ice is warmer, which creates a system with a cold and strong layer at the top and a warmer and softer layer at the bottom. Shortening of individual layers with small-scale viscosity contrasts could potentially lead to buckle folding, as has been suggested by NEEM-community (2013). Initial wavelengths for low viscosity contrasts would be at least five to 10 times the layer thickness (Llorens et al., 2013; Schmalholz & Mancktelow, 2016), which in our case would be at least 5–10 km. However, the viscosity contrast between the warm and cold ice is relatively low and lacks a sharp boundary. Although the resulting wavelengths are in the same order as those of folds observed in the ice sheets, the amplification rate is very small (Llorens et al., 2013) and no visible folds are expected to form. These theoretical considerations, modeling by Bons et al. (2016), as well as the results of Models 1–3 (no bedrock bumps) and isotropic Model 15 (Figure S12 in Supporting Information S1), indicate that Biot-type buckle folding due to viscosity contrasts between cold and warm ice cannot lead to significant folding on the multi-km scale.

Deformation in the deepest, softest ice is approximately in simple shear. In case of bedrock bumps, the basal shear zone may localize above the bedrock-ice interface, especially across valleys or downstream of bumps in the bedrock (Figure 3g; Liu et al., 2024). This effect is more pronounced in case of anisotropy (Sachau et al., 2022). Passive shearing of layers in heterogeneous simple shear leads to tight recumbent folds (Figures 3c and 3f) that are also observed in ice sheets (Figure 1e; Bons et al., 2016). Recumbent folds may be enhanced by anisotropy, but are largely controlled by the deep bed-parallel shearing and bedrock topography, not by anisotropy. Connection of the deep recumbent folds with a shallowly dipping axial plane with more upright folds higher up in the ice leads to the listric shape of the axial planes (Franke, Bons, et al., 2022). Variable bed conditions, for example, enabling bed sliding, are expected to further enhance folding in the ice basal layers (Leysinger Vieli et al., 2018; Wolovick & Creyts, 2016).

Our simulations with anisotropic ice properties appear to successfully explain large-scale folding in convergent flow especially near ice streams. The mechanism of fold amplification due to anisotropy and buoyancy is not competing with other proposed mechanisms for the formation of large, often recumbent, folds (e.g., Leysinger Vieli et al., 2018; Wolovick et al., 2014), but, instead, would act together with these to create even taller folds. Precipitation on the ice-sheet surface would, on the other hand, suppress fold amplification (Waddington et al., 2001), although our simulations show that significant fold amplitudes can still be attained within 3,000 years with a moderate surface accumulation (Figure S11 in Supporting Information S1).

Fold amplification due to anisotropy or basal processes is to a large extent independent of the effective ice viscosity, but depends more on the kinematics of flow (e.g., convergent flow) or the rates of basal processes (e.g., basal freeze-on; Leysinger Vieli et al., 2018). Effective viscosity is, however, critical for the effect of buoyancy of the deepest and warmest ice (Hughes, 2009). Our simulations (Model 6; Figure 4a) indicate that fold amplification can be significantly enhanced to form tall "plume-like" folds, when the overall flow velocity is sufficiently high to reduce the effective viscosity enough to allow the rise of warm, buoyant ice in anticlinal cores. Our first results on the effect on buoyancy indicate that much more work is needed, as well as the need to constrain the effective viscosity of flowing ice.

5. Conclusions

Motivated by observations of folds in radargrams of the GrIS, our modeling results show that: (a) Large-scale folds can form in convergent ice flow, mainly controlled by its rheological anisotropy. This anisotropy is due to the CPO. Anisotropy amplifies existing undulations in the ice stratigraphy due to bedrock topography or processes at the ice-bed interface. (b) Rheological variations within the ice sheet, such as vertical viscosity gradients that result from temperature gradients in ice layers, appear to not play a significant role. (c) Buoyancy of the deepest and warmest ice in anticlinal cores can significantly enhance fold amplifications where ice is effectively weakened by strain-rate softening due to the power-law rheology of ice. (d) As observed in ice sheets, large-scale fold amplitudes are highest in the middle of the ice column or just below. Meanwhile, near-base fold patterns are more complex and often result in recumbent folds due to the bedrock constraint. (e) Small-scale folds on initially flat internal horizons may form as well due to the anisotropy of ice. Finally, using particle tracking and strain analysis, our modeling helps to better explain ice-flow dynamics of ice sheets. In particular, an improved implementation of ice anisotropy and basal shearing can result in high-strain-rate areas where the power-law ice would be softened, even when frozen to the bed. This indicates that ice sheets could be more unstable when

suddenly triggered to flow by external forcings, such as climate change, ice-sheet geometry changes or tectonic events.

Data Availability Statement

Underworld is fully open-source and the version (v2.14.1b) used for this paper is available through Beucher et al. (2022). Our code files for all the models are available through Zhang (2024). The radio-echo sounding data shown in Figure 1c (profile IDs: 20180509_01_[011, 012]) and in Figure 1f (profile ID: 20180512_02_009) from AWI's EGRIP-NOR-2018 survey are available under https://doi.org/10.1594/PANGAEA.928569 (Franke, Jansen, et al., 2022), the data shown in Figure 1d (profile ID: 20110507_01_032) is available via the CReSIS Data Products (https://data.cresis.ku.edu/) and the data shown in Figure 1e (profile ID: 20180415_06_007) is available under https://doi.org/10.1594/PANGAEA.949391 (Franke, Bons, et al., 2022). Bed elevation data from Morlighem et al. (2017) and ice flow velocity data from Joughin et al. (2018) are available at the National Snow and Ice Data Center: https://nsidc.org/data/idbmg4 and https://nsidc.org/data/nsidc-0670/, respectively.

Acknowledgments
Yu Zhang was funded by the China Scholarship Council (Grant number 202006010063) recommended by Peking Univesity, and Steven Franke by the Walter Benjamin Programme of the Deutsche Forschungsgemeinschaft (DFG, German Research Foundation; project number 506043073). We acknowledge support from the Open Access Publication Fund of the University of Tübingen. We thank the editor Mathieu Morlighem as well as Michael Wolovick, Peter Hudleston, and Dave Prior for their comments that helped to improve the text. Open Access funding enabled and organized by Projekt DEAL.

References

Alley, R. B., Gow, A. J., Meese, D. A., Fitzpatrick, J. J., Waddington, E. T., & Bolzan, J. F. (1997). Grain-scale processes, folding, and stratigraphic disturbance in the GISP2 ice core. *Journal of Geophysical Research*, *102*(C12), 26819–26830. https://doi.org/10.1029/96JC03836

Bell, R. E., Tinto, K., Das, I., Wolovick, M., Chu, W., Creyts, T. T., et al. (2014). Deformation, warming and softening of Greenland's ice by refreezing meltwater. *Nature Geoscience*, *7*(7), 497–502. https://doi.org/10.1038/ngeo2179

Beucher, R., Giordani, J., Moresi, L., Mansour, J., Kaluza, O., Velic, M., et al. (2022). Underworld2: Python geodynamics modelling for desktop, HPC and cloud (v2.14.1b) [Software]. *Zenodo*. https://doi.org/10.5281/zenodo.7455999

Biot, M. A. (1957). Folding instability of a layered viscoelastic medium under compression. *Proceedings of the Royal Society of London - Series A: Mathematical and Physical Sciences*, *242*(1231), 444–454. https://doi.org/10.1098/rspa.1957.0187

Bons, P. D., Jansen, D., Mundel, F., Bauer, C. C., Binder, T., Eisen, O., et al. (2016). Converging flow and anisotropy cause large-scale folding in Greenland's ice sheet. *Nature Communications*, *7*(1), 11427. https://doi.org/10.1038/ncomms11427

Duval, P., Ashby, M. F., & Anderman, I. (1983). Rate-controlling processes in the creep of polycrystalline ice. *Journal of Physical Chemistry A*, *87*(21), 4066–4074. https://doi.org/10.1021/j100244a014

Franke, S., Bons, P. D., Streng, K., Mundel, F., Binder, T., Weikusat, I., et al. (2023). Three-dimensional topology dataset of folded radar stratigraphy in northern Greenland. *Scientific Data*, *10*(1), 525. https://doi.org/10.1038/s41597-023-02339-0

Franke, S., Bons, P. D., Westhoff, J., Weikusat, I., Binder, T., Streng, K., et al. (2022). Holocene ice-stream shutdown and drainage basin reconfiguration in northeast Greenland. *Nature Geoscience*, *15*(12), 995–1001. https://doi.org/10.1038/s41561-022-01082-2

Franke, S., Jansen, D., Binder, T., Paden, J. D., Dörr, N., Gerber, T. A., et al. (2022). Airborne ultra-wideband radar sounding over the shear margins and along flow lines at the onset region of the Northeast Greenland Ice Stream. *Earth System Science Data*, *14*(2), 763–779. https://doi.org/10.5194/essd-14-763-2022

Gillet-Chaulet, F., Gagliardini, O., Meyssonnier, J., Zwinger, T., & Ruokolainen, J. (2006). Flow-induced anisotropy in polar ice and related ice-sheet flow modelling. *Journal of Non-Newtonian Fluid Mechanics*, *134*(1–3), 33–43. https://doi.org/10.1016/j.jnnfm.2005.11.005

Goldsby, D. L., & Kohlstedt, D. L. (2001). Superplastic deformation of ice: Experimental observations. *Journal of Geophysical Research*, *106*(B6), 11017–11030. https://doi.org/10.1029/2000JB900336

Hudleston, P. J. (2015). Structures and fabrics in glacial ice: A review. *Journal of Structural Geology*, *81*, 1–27. https://doi.org/10.1016/j.jsg.2015.09.003

Hughes, T. (2009). Thermal convection and the origin of ice streams. *Journal of Glaciology*, *55*(191), 524–536. https://doi.org/10.3189/002214309788816722

Jansen, D., Franke, S., Bauer, C. C., Binder, T., Dahl-Jensen, D., Eichler, J., et al. (2024). Shear margins in upper half of Northeast Greenland Ice Stream were established two millennia ago. *Nature Communications*, *15*(1), 1193. https://doi.org/10.1038/s41467-024-45021-8

Jansen, D., Llorens, M. G., Westhoff, J., Steinbach, F., Kipfstuhl, S., Bons, P. D., et al. (2016). Small-scale disturbances in the stratigraphy of the NEEM ice core: Observations and numerical model simulations. *The Cryosphere*, *10*(1), 359–370. https://doi.org/10.5194/tc-10-359-2016

Jennings, S. J. A., & Hambrey, M. J. (2021). Structures and deformation in glaciers and ice sheets. *Reviews of Geophysics*, *59*(3), e2021RG000743. https://doi.org/10.1029/2021RG000743

Joughin, I. A. N., Smith, B. E., & Howat, I. M. (2018). A complete map of Greenland ice velocity derived from satellite data collected over 20 years. *Journal of Glaciology*, *64*(243), 1–11. https://doi.org/10.1017/jog.2017.73

Kocher, T., Mancktelow, N. S., & Schmalholz, S. M. (2008). Numerical modelling of the effect of matrix anisotropy orientation on single layer fold development. *Journal of Structural Geology*, *30*(8), 1013–1023. https://doi.org/10.1016/j.jsg.2008.04.006

Krabbendam, M. (2016). Sliding of temperate basal ice on a rough, hard bed: Creep mechanisms, pressure melting, and implications for ice streaming. *The Cryosphere*, *10*(5), 1915–1932. https://doi.org/10.5194/tc-10-1915-2016

Kuiper, E. J. N., De Bresser, J. H., Drury, M. R., Eichler, J., Pennock, G. M., & Weikusat, I. (2020). Using a composite flow law to model deformation in the NEEM deep ice core, Greenland–Part 2: The role of grain size and premelting on ice deformation at high homologous temperature. *The Cryosphere*, *14*(7), 2449–2467. https://doi.org/10.5194/tc-14-2449-2020

Leysinger Vieli, G. M., Martin, C., Hindmarsh, R. C. A., & Lüthi, M. P. (2018). Basal freeze-on generates complex ice-sheet stratigraphy. *Nature Communications*, *9*(1), 4669. https://doi.org/10.1038/s41467-018-07083-3

Liu, E. W., Räss, L., Herman, F., Podladchikov, Y., & Suckale, J. (2024). Spontaneous formation of an internal shear band in ice flowing over topographically variable bedrock. *Journal of Geophysical Research: Earth Surface*, *129*(4), e2022JF007040. https://doi.org/10.1029/2022JF007040

Llorens, M. G., Bons, P. D., Griera, A., Gomez-Rivas, E., & Evans, L. A. (2013). Single layer folding in simple shear. *Journal of Structural Geology*, *50*, 209–220. https://doi.org/10.1016/j.jsg.2012.04.002

MacGregor, J. A., Fahnestock, M. A., Catania, G. A., Paden, J. D., Prasad Gogineni, S., Young, S. K., et al. (2015). Radiostratigraphy and age structure of the Greenland ice sheet. *Journal of Geophysical Research: Earth Surface*, *120*(2), 212–241. https://doi.org/10.1002/2014JF003215

Martín, C., Gudmundsson, G. H., Pritchard, H. D., & Gagliardini, O. (2009). On the effects of anisotropic rheology on ice flow, internal structure, and the age-depth relationship at ice divides. *Journal of Geophysical Research*, *114*(F4). https://doi.org/10.1029/2008JF001204

Morlighem, M., Williams, C. N., Rignot, E., An, L., Arndt, J. E., Bamber, J. L., et al. (2017). BedMachine v3: Complete bed topography and ocean bathymetry mapping of Greenland from multibeam echo sounding combined with mass conservation. *Geophysical Research Letters*, *44*(21), 11–051. https://doi.org/10.1002/2017GL074954

NEEM community members. (2013). Eemian interglacial reconstructed from a Greenland folded ice core. *Nature*, *493*(7433), 489–494. https://doi.org/10.1038/nature11789

Panton, C., & Karlsson, N. B. (2015). Automated mapping of near bed radio-echo layer disruptions in the Greenland Ice Sheet. *Earth and Planetary Science Letters*, *432*, 323–331. https://doi.org/10.1016/j.epsl.2015.10.024

Ran, H., de Riese, T., Llorens, M. G., Finch, M. A., Evans, L. A., Gomez-Rivas, E., et al. (2019). Time for anisotropy: The significance of mechanical anisotropy for the development of deformation structures. *Journal of Structural Geology*, *125*, 41–47. https://doi.org/10.1016/j.jsg.2018.04.019

Robin, G. D. Q. (1955). Ice movement and temperature distribution in glaciers and ice sheets. *Journal of Glaciology*, *2*(18), 523–532. https://doi.org/10.3189/002214355793702028

Rogozhina, I., Martinec, Z., Hagedoorn, J. M., Thomas, M., & Fleming, K. (2011). On the long-term memory of the Greenland Ice Sheet. *Journal of Geophysical Research*, *116*(F1). https://doi.org/10.1029/2010JF001787

Sachau, T., Yang, H., Lang, J., Bons, P. D., & Moresi, L. (2022). ISMIP-HOM benchmark experiments using Underworld. *Geoscientific Model Development*, *15*(23), 8749–8764. https://doi.org/10.5194/gmd-15-8749-2022

Schmalholz, S. M., & Mancktelow, N. S. (2016). Folding and necking across the scales: A review of theoretical and experimental results and their applications. *Solid Earth*, *7*(5), 1417–1465. https://doi.org/10.5194/se-7-1417-2016

Sharples, W., Moresi, L. N., Velic, M., Jadamec, M. A., & May, D. A. (2016). Simulating faults and plate boundaries with a transversely isotropic plasticity model. *Physics of the Earth and Planetary Interiors*, *252*, 77–90. https://doi.org/10.1016/j.pepi.2015.11.007

Thorsteinsson, T., & Waddington, E. D. (2002). Folding in strongly anisotropic layers near ice-sheet centers. *Annals of Glaciology*, *35*, 480–486. https://doi.org/10.3189/172756402781816708

Waddington, E. D., Bolzan, J. F., & Alley, R. B. (2001). Potential for stratigraphic folding near ice-sheet centers. *Journal of Glaciology*, *47*(159), 639–648. https://doi.org/10.3189/172756501781831756

Wolovick, M. J., & Creyts, T. T. (2016). Overturned folds in ice sheets: Insights from a kinematic model of traveling sticky patches and comparisons with observations. *Journal of Geophysical Research: Earth Surface*, *121*(5), 1065–1083. https://doi.org/10.1002/2015JF003698

Wolovick, M. J., Creyts, T. T., Buck, W. R., & Bell, R. E. (2014). Traveling slippery patches produce thickness-scale folds in ice sheets. *Geophysical Research Letters*, *41*(24), 8895–8901. https://doi.org/10.1002/2014GL062248

Zhang, Y. (2024). Underworld modeling of large-scale folds in ice sheets. *Zenodo*. https://doi.org/10.5281/zenodo.11396618

References From the Supporting Information

Bons, P. D., Kleiner, T., Llorens, M. G., Prior, D. J., Sachau, T., Weikusat, I., & Jansen, D. (2018). Greenland Ice Sheet: Higher nonlinearity of ice flow significantly reduces estimated basal motion. *Geophysical Research Letters*, *45*(13), 6542–6548. https://doi.org/10.1029/2018GL078356

Fuchs, L., Schmeling, H., & Koyi, H. (2011). Numerical models of salt diapir formation by down-building: The role of sedimentation rate, viscosity contrast, initial amplitude and wavelength. *Geophysical Journal International*, *186*(2), 390–400. https://doi.org/10.1111/j.1365-246X.2011.05058.x

Gillet-Chaulet, F., Gagliardini, O., Meyssonnier, J., Montagnat, M., & Castelnau, O. (2005). A user-friendly anisotropic flow law for ice-sheet modeling. *Journal of Glaciology*, *51*(172), 3–14. https://doi.org/10.3189/172756505781829584

Hills, B. H., Harper, J. T., Humphrey, N. F., & Meierbachtol, T. W. (2017). Measured horizontal temperature gradients constrain heat transfer mechanisms in Greenland ice. *Geophysical Research Letters*, *44*(19), 9778–9785. https://doi.org/10.1002/2017GL074917

Marion, G. M., & Jakubowski, S. D. (2004). The compressibility of ice to 2.0 kbar. *Cold Regions Science and Technology*, *38*(2–3), 211–218. https://doi.org/10.1016/j.coldregions.2003.10.008

Moresi, L., & Mühlhaus, H. B. (2006). Anisotropic viscous models of large-deformation Mohr–Coulomb failure. *Philosophical Magazine*, *86*(21–22), 3287–3305. https://doi.org/10.1080/14786430500255419

Moresi, L., Dufour, F., & Mühlhaus, H. B. (2003). A Lagrangian integration point finite element method for large deformation modeling of viscoelastic geomaterials. *Journal of Computational Physics*, *184*(2), 476–497. https://doi.org/10.1016/S0021-9991(02)00031-1

Pattyn, F., Perichon, L., Aschwanden, A., Breuer, B., De Smedt, B., Gagliardini, O., et al. (2008). Benchmark experiments for higher-order and full-Stokes ice sheet models (ISMIP–HOM). *The Cryosphere*, *2*(2), 95–108. https://doi.org/10.5194/tc-2-95-2008

Pettit, E. C., Waddington, E. D., Harrison, W. D., Thorsteinsson, T., Elsberg, D., Morack, J., & Zumberge, M. A. (2011). The crossover stress, anisotropy and the ice flow law at Siple Dome, West Antarctica. *Journal of Glaciology*, *57*(201), 39–52. https://doi.org/10.3189/002214311795306619

Vollmer, F. W. (2024). Orient: Directional data analysis software. https://vollmerf.github.io/orient/